

ENHANCED STRUCTURAL AND OPTICAL PROPERTIES OF ZnO NANOPARTICLES UNDER DIFFERENT SUBSTITUTIONS SYNTHESIZED BY CO-PRECIPIATION TECHNIQUE

A. SATTAR^a, K. ALI^{b,*}, M. SAJJAD^b, M. Z. SHOUKAT^a, U. ISHTIAQ^a,
S. U. REHMAN^a, A. RIZWAN^d, A. SUHALE^b, K. ARSHAD^a, C. M. NOUMAN^a,
A. B. MUJAHID^a, M. SYAM^a, M. M. JOIYA^c

^aDepartment of Mechanical, Mechatronics, and Manufacturing Engineering (New Campus KSK), University of Engineering and Technology, Lahore, Pakistan

^bNano-optoelectronics Research Laboratory, Department of Physics, University of Agriculture Faisalabad, 38040 Faisalabad, Pakistan

^cDepartment of Biomedical engineering (New Campus KSK), University of Engineering and Technology, Lahore, Pakistan

^dDepartment of Chemical, Polymer and Composite material Engineering (New Campus KSK) University of Engineering and Technology Lahore, Pakistan

Nano-crystalline particles of zinc oxide having different concentration (0.001, 0.002, 0.003) were effectively synthesized via Co-precipitation technique. Increasing the concentration of Zinc, lattice parameter (a) and (c) of crystal lattice increases according to Vegard's Law. Phase identification of ZnO nanoparticle was analyzed via X-ray diffraction (XRD) and absorbance was measured by ultraviolet visible (UV) spectroscopy. Increment of band gap energy values by increasing concentration of Zinc (Zn^{2+}) ions. An absorbance spectrophotometer was utilized to measure the amount of light passing through differently zinc concentrated solutions. The Absorption peak at 370nm was observed. When concentration increases, peak of absorption displays a progressive red shift. The subsequent redshifts, as stated earlier, are consistent with the observed variance in NP sizes. Fourier transform infrared (FTIR) spectra of zinc nanoparticles were investigated in the spectral region of $4000-500\text{ cm}^{-1}$. ZnO samples morphology were also analyzed using scanning electron microscope (SEM). Particles with identical and significant tendency of metallic cluster were observed throughout the samples.

(Received May 4, 2020; Accepted August 11, 2020)

Keywords: ZnO, Nanoparticles, XRD, SEM, FTIR, Optical properties, Vegard's Law, Band gap energy

1. Introduction

The reason behind the inquisitiveness of ZnO among research community is due to its high excitation-binding energy as much as 60 meV. It may result a lasting action whose base is excitation temperature[1]. Nanocrystalline materials research is enormously increased from the few years. Practical applications are of great consideration for new materials. High catalytic activity and large surface area of ZnO is the reason for their application to catalytic processes. ZnO nanoparticles applications comprise in preparing, chemical absorbent varistors[2,3], gas sensors[4,5], optical devices and electrical [6-8], solar cell [9], catalysts for liquid phase hydrogenation [10], catalysts for photo-catalytic degradation [11-13] and instead of titanium nanoparticles[14-17], electrostatic dissipative coating[18]. As a consequence of modification and synthesis, nanosized ZnO have concerned considerable interest. Some synthesis procedures are microemulsion synthesis[19], mechanochemical processing[20], including sol-gel technique[21,22], spray pyrolysis and drying[13,23], RF plasma synthesis[24], supercritical-water

* Corresponding author: khuram_uaf@yahoo.com

processing[25], thermal decomposition of organic precursor[26], hydrothermal processing[27, 28], microwave-assisted synthesis or sonochemical [29,30], vapor transport process[31], or self-assembling[32], homogeneous precipitation [33,34]and direct precipitation[35]. Because of its outstanding characteristics, nano-material being substantially different from microparticle equivalents, has gained considerable interest, primarily due to the finite-size effect and high surface-to-volume ratio. The production of nano sized ZnO which includes thermal decomposition, chemical vapor deposition, spray pyrolysis, precipitation. Their production is in accordance with uniform size and morphology. But precipitation approach is the simplified one and more suitable for large scale production. Photoconductivity and high transparency can also be observed by zinc oxide nanoparticles in visible light. That's why in solar cell, they can be used as transparent electrodes. Doping of zinc oxide with some transition metals enhances its optical and magneto-optical properties. Properties tuning of ZnO requires controlling of different parameters in chemical synthesis such as metal concentration, stirring time, base solution, heating time. Researchers have tried to manipulate these parameters to obtain desired properties of ZnO but there is still space left for fine tuning of the structures with appropriate properties and enough high yield. In this new work, Co-precipitation method was used to the prepare ZnO nanoparticles (NPs) under different zinc substitution, sodium hydroxide was used as precipitating agent and it serves as a terminator for growing the ZnO nanoparticles (NPs) because of the particles cannot come together easily and it expands during the calcination process. The size, crystallinity and morphology of the resulting ZnO-NPs were studied. Keeping this in mind, we have designed this study to synthesize ZnO nanoparticles with different zinc precursor concentration and studied its effect on structural, morphological and optical properties.

2. Experimental

During experiment, Zinc sulphate dehydrate ($\text{ZnSO}_4 \cdot 2\text{H}_2\text{O}$), sodium hydroxide pellets and distilled water was used. All analytical grade samples used in the preparation of material were purchased from (Merck and Sigma Aldrich through local suppliers) in pure form without any need of further purification.

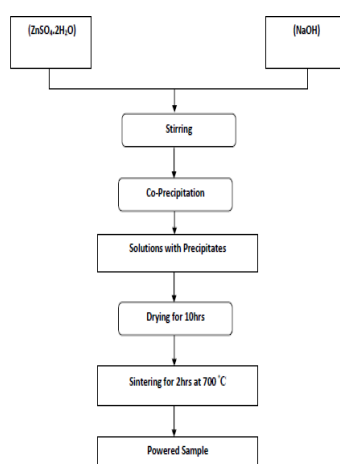


Fig. 1. The schematic flow chart to exhibits the (0.001, 0.002, 0.003) grams for ZnO Nano-particles samples.

A standard procedure was adopted to synthesize ZnO nanoparticles. During synthesis (0.001, 0.002, 0.003) grams of Zinc sulphate dehydrate ($\text{ZnSO}_4 \cdot 2\text{H}_2\text{O}$) were used for synthesized of ZnO and required amount of NaOH pellets were dissolved in distilled water. In the current research work, zinc oxide nanoparticles were synthesized via Co-precipitation method. At room temperature, in solution of $\text{ZnSO}_4 \cdot 2\text{H}_2\text{O}$, NaOH was added dropwise under constant stirring. The

solution was mixed with precipitating agent (NaOH) to obtain less chemically dispersed nanoparticles. The solution color was gradually changed black to white and finally white while the reaction proceeded. The pH 11 was maintained throughout the reaction. The stirring was stopped as pH approached at 11, after that sample had kept for aging for 10 hours. The precipitates present in the solution settled down after the completion of reaction process. After becoming the precipitate, Samples were washed with distilled water several times to reduce contamination and unwanted impurity until pH become neutral. For 10 hours the specimen was dried at 80°C. Dried sample was grinded carefully obtain powder sample. In order to obtain crystalline ZnO nanoparticles the dried samples were calcinated in furnace at 700°C temperature for 2 hours. The schematic flow chart of ZnO nano-particles (NPs) as shown in figure 1. All prepared samples of ZnO Nano-particles have characterized by X-ray diffraction, UV-vis spectroscopy to study their UV spectra, Scanning electron microscopy, particle structure and morphology and FTIR spectrum, functional groups respectively.

3. Results and discussion

Crystalline size (D) is measured in nano-meter. Lambda (λ) is the X-ray wavelength having a typical value of about 1.54Å. Shape factor (K) having a typical value of approximately (0.9-0.99) fluctuate with the definite shape of the crystallites.

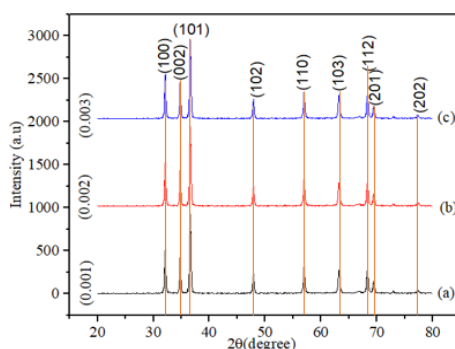


Fig. 1 XRD pattern ZnO having zinc concentrations (0.001, 0.002, 0.003).

As the Fig. 2 represents that XRD pattern of ZnO particles. The XRD peaks of the definite boarding peaks that prepared material consist particles at nanoscale. of data. Diffraction peaks of fig.2(a-c) are indexed to (100), (002), (101), (102), (110), (103), (112), (201) and (202) reflection angle at 2θ values 32.20, 34.87, 36.75, 47.81, 57.03, 63.31, 68.24, 69.44 and 77.32 respectively. XRD The XRD Pattern give the peak intensity, full width half maxima (FWHM) and positions diffraction pattern of specimen showed the development of hexagonal wurtzite structure and purity of the phase of ZnO. XRD analysis peaks perfectly matched with the JCPDS Card # 36-1451 suggesting purity of hexagonal wurtzite structure. No additional peaks detected in figure; 2(a-c), it ascribes contamination phases in ZnO samples. High intensity of sharp diffraction peaks appeared at 36.75 indexed to (101) plane is indicate to be measured of its perfect crystallinity. Average crystalline size (D) is formulated via XRD analysis for different diffractions angle by using Scherrer's equation.

Average crystalline size (D) is calculated via XRD analysis for different diffraction angle by using Scherr's equation.

$$D = \frac{0.9\lambda}{\beta \cos\theta} \quad (1)$$

where " λ " is X-ray wavelength, " β " is full width half maxima and " θ " is angle of X-ray diffraction.

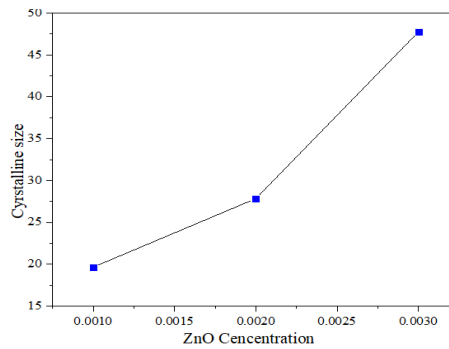


Fig. 2. Graph plotted of Zn concentration against Crystalline size.

Crystalline size (Dnm) were calculated via Scherrer's equation. Graph plotted between the ZnO concentration against crystalline size shown in Fig. 3. The average particle size has been evaluated at ZnO concentrations are found 19.64, 27.83 and 47.75nm respectively shown in Table 1.

As the lattice constant can be calculated via following equation

$$\frac{1}{d^2} = \frac{4}{3} \left(\frac{h^2 + hk + k^2}{a^2} \right) + \frac{l^2}{c^2} \quad (2)$$

where "d" is the de-spacing, "h,k,l" is the miller indices, "a" and "c" is the length of crystal.

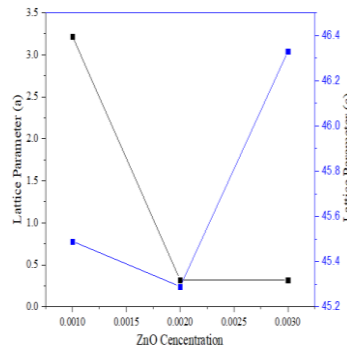


Fig. 3. Graph plotted of Zn concentration against Lattice parameter (a, c).

In Fig. 4 by increasing the concentration of Zinc ion, lattice parameter (a) and (c) of crystal lattice increases according to heuristic Vegard's Law[36]. Increase in the lattice constant (a) and (c) linearly by increasing the concentration of zinc ion (Zn^{2+}) specifies the enlargement of crystal lattice without any change in the regularity of crystal lattice. Increase in the crystal lattice constant occur due to the bigger size of zinc ions (Zn^{2+}) having ionic radius of (0.82 Å)

The Volume (V) also be calculated via following formula.

$$V = \frac{\sqrt{3}}{2} a^2 c \quad (3)$$

where "a" and "c" are the lattice constant.

Dislocation density has been calculated from the following formula.

$$\rho = \frac{1}{D^2} \quad (4)$$

where “D” is the average crystalline size.

Here, we can calculate the number of unit cell from the following equation.

$$n = \pi \times \left(\frac{4}{3}\right) \times \left(\frac{D}{2}\right) \times \left(\frac{1}{V}\right) \quad (5)$$

where “n” is the number of unit cell, “D” is average crystalline size and “V” is volume of the unit cell.

Morphology index can also be calculated from the following relation

$$M. I = \frac{FWHM_h}{FWHM_h + FWHM_p} \quad (6)$$

where (M.I) is morphology Index, $FWHM_h$ is the high peak and $FWHM_p$ is the particular peaks.

Density can be measured by the following formula

$$\text{Density } (\rho_x) = \frac{nM_w}{N_A V} \quad (7)$$

where n is number of atoms per unit cell, M_w is molecular weight, N_A is Avogadro number having value $6.02214076 \times 10^{23}$ and V is the volume of unit cell.

Table 1. Zn Concentration, Crystalline size (Dnm), Volume (V), Dislocation density (ρ), Number of atoms (n), Morphology Index (M.I), X-ray density (ρ_x) calculated from XRD of different samples.

concentration	D(nm)	Lattice Constant A=b \neq c		Volume	Dislocation density (ρ)	Number of Atoms (n)	Morphology Index (M.I)	Density (ρ_x)
		a	c					
0.001	19.64	03.22	0.516	45.49	0.002592	0.904	0.5001	4.485×10^{23}
0.002	27.83	0.319	0.514	45.29	0.001291	1.286	0.6362	4.466×10^{23}
0.003	47.75	0.320	0.513	46.33	0.0004385	2.158	0.6761	4.438×10^{23}

The particle size and lattice strain of Zn doped Cobalt ferrite samples were calculated via broadening of the XRD peaks using Williamson-Hall method from the following relation.

$$\beta \cos \theta = \frac{k\lambda}{D} + 4\epsilon \sin \theta \quad (8)$$

Here, β is represented the integral breadth in radian, θ is Bragg angle in radian, k is shape value 0.94, D is the William hall particles size (D_{H-W}) and ϵ stand for micro slop. The calculated lattice strains from W-H plot were found be decrease with decreasing ZnO-concentration which is presented in table 2. The William plot of all ZnO samples is shown in Fig. 4.

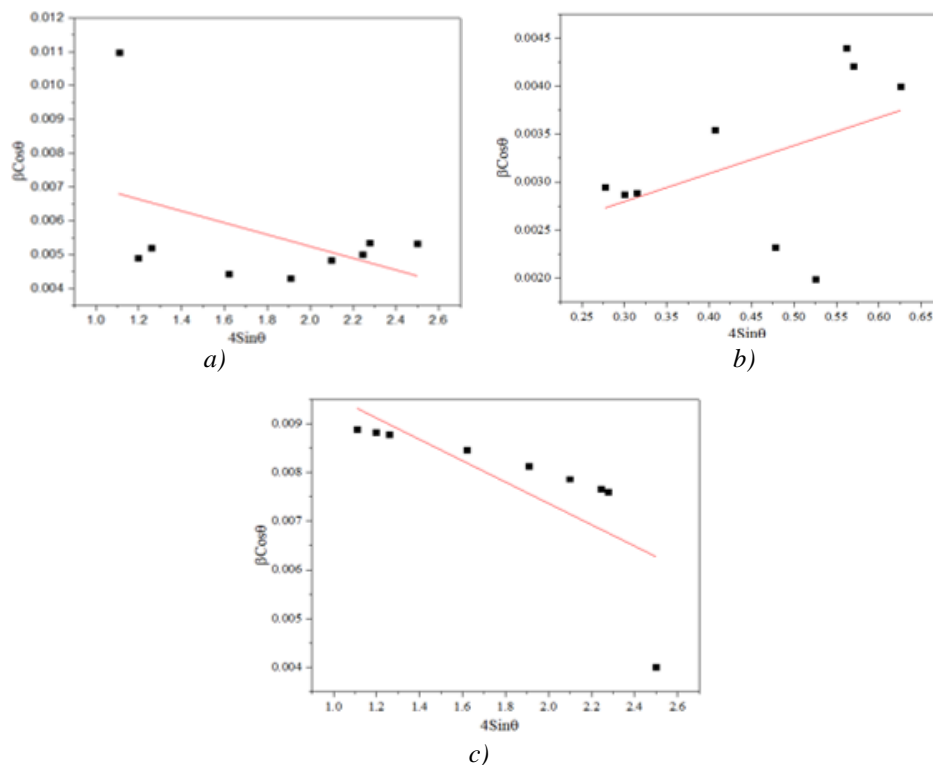


Fig. 4. Hall-Williamson plot of ZnO Concentration (a)0.001(b)0.002 (c) 0.003.

In order to estimate the slop of linear fit data plotted against $4\text{Sin}\theta$ vis $\beta\text{Cos}\theta$, gives the information about the inverse of intercept and lattice strain gives the value of crystalline size ($D_{\text{W-H}}$) for all the ZnO samples shows in figure 5. As the ZnO concentration is increased the crystalline size calculated from the Williamsons hall method is increased. The value of strain (ϵ) is also increased by increasing the ZnO concentrations as shown in Fig. 6.

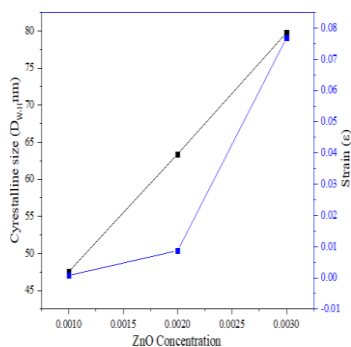


Fig. 5. Graph plotted of ZnO concentration against Crystalline Size ($D_{\text{W-H}}$) and Strain(ϵ).

Table 2. ZnO Concentration, Crystalline size (D_{nm}) from Williamsons Hall method and strain were calculated from XRD of different samples.

Concentration	$D_{\text{H-W}}$ (nm)	Strain (ϵ)
0.001	47.52	0.00073022
0.002	63.41	0.00873
0.003	79.74	0.0768

Electron microscopy generates high-resolution images and the features and objects can be observed precisely. Evolution of identical particles, significant tendency of metallic cluster and growth can be observed clearly. Surface topography as well as the composition of ZnO samples can also be measured. Through SEM, we can achieve resolution up to more than one nanometer. SEM micrographs of prepared ZnO nanoparticles shown in figure 7. ZnO samples gives the nanowire shown in Fig. 7. From given micrographs, the presence of agglomeration was confirmed.

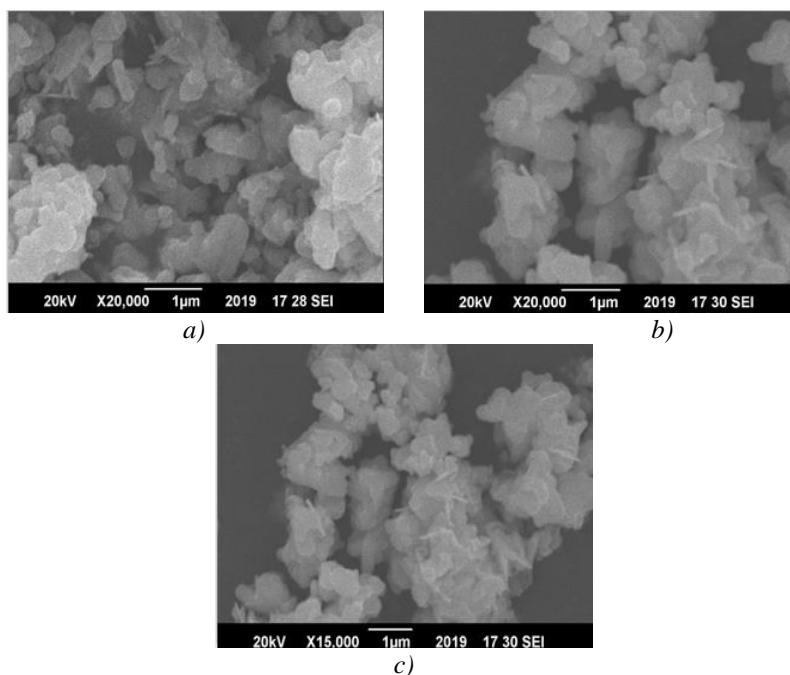


Fig. 6. SEM micrographs of ZnO having concentrations (a) 0.001 (b) 0.002 (c) 0.003.

Calculated average grain size of ZnO nano particles prepared by Co-Precipitation method is 31.53nm, 32.87nm and 41.44nm respectively. The sintering of the ZnO appears to be significantly different from pure material. As the concentration were increased the grain size of the SEM images also increased as shown in Fig. 8.

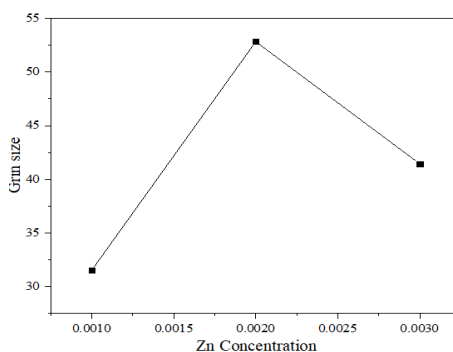


Fig. 7. Graph plotted of ZnO concentration against grain size.

Fourier transform infrared spectra (FT-IR) is an analysis which generates an infrared radiation spectrum of absorption of material. The IR spectroscopy is a versatile tool for identification of purity, functional groups and phase of samples. In Fig. 9 FT-IR spectra of ZnO hexagonal wurtzite structure are reported in the region of $4000\text{-}500\text{cm}^{-1}$. Obtained FTIR spectra of ZnO NPs demonstrates prominent peaks at $3441, 1636, 1343, 1106$ and 635 cm^{-1} . To be more

specific, a broad band round about at 3500 cm^{-1} is assigned to O-H stretching mode of hydroxyl group. Broad vibrational band observed at 3441 cm^{-1} is attributed to symmetric stretching mode of water molecules. Band at 1636 is allocated to bending vibrational mode of water molecules. Peak at 1107 cm^{-1} infers a triply degenerate symmetric stretching mode of SO_4^{2-} . Absorption band of low frequency is noticed above 600 cm^{-1} in ZnO hexagonal wurtzite structure.

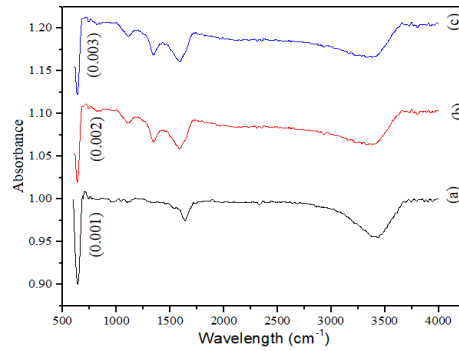


Fig. 8. IR spectrum of ZnO having concentrations (a) 0.001 (b) 0.002 (c) 0.003.

Fig. 10 shows the absorption spectrum of Zinc oxide for different concentrations of Zinc (Zn^{2+}) ions. The result of UV Spectra indicate that specimen had symbolic absorbance in the range of 300-900 nm. Fig. 10 demonstrates optical absorption of ZnO nanoparticles. Absorption peak is at 370 nm. When concentration increases, peak of absorption displays a progressive red shift. The subsequent redshifts, as stated earlier, are consistent with the observed variance in NP sizes. The estimated values of band gap energy of the specimens of Zinc Oxide are extracted from a plot of $(\alpha h\nu)^2$ against energy of photon ($h\nu$).

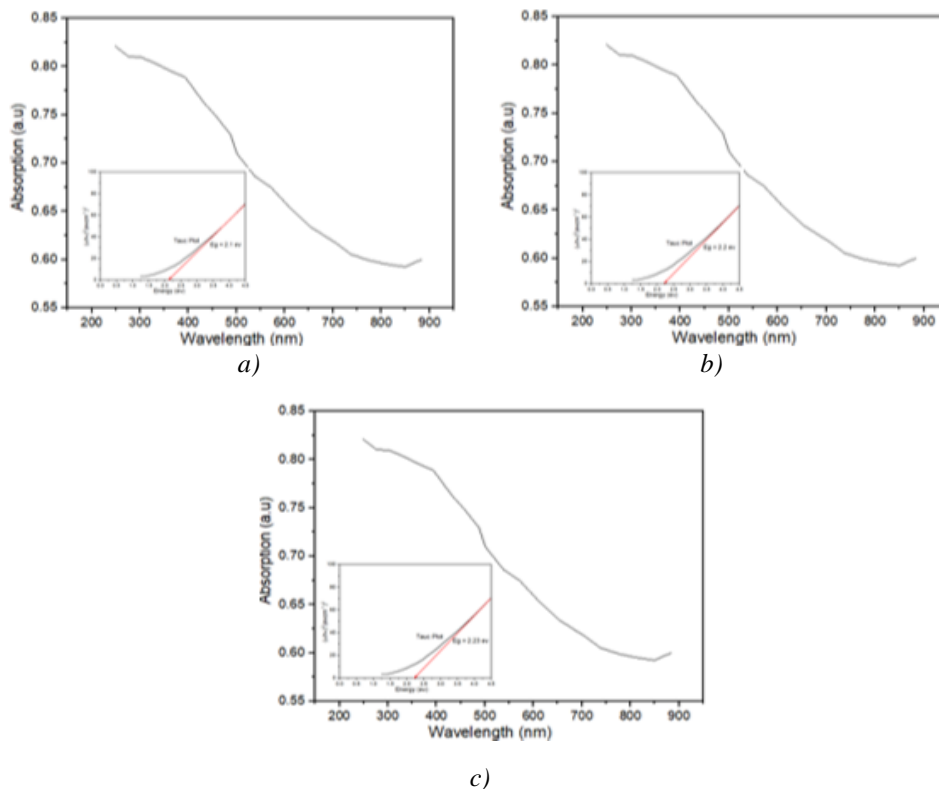


Fig. 9. Uv spectroscopy of ZnO having concentrations (a) 0.001 0.002 (c)0.003.

The coefficient of optical absorption near the band edge is calculated from Tauc relation using following equation:

$$\alpha h\nu = A(h\nu - E_g) \quad (9)$$

where h is Plank's constant, ν is frequency of incident photon, α is absorption coefficient, A is a constant, n depends on nature of transition ($n = 1$ for direct transition) and E_g is optical energy direct band gap and α is the absorption coefficient calculation formula is:

$$a = 2.303\left(\frac{Ab}{t}\right) \quad (10)$$

Intercept of tangent of $(\alpha h\nu)^2$ and the $(h\nu)$ is photon energy are used for band gap calculation. The gap obtained from ZnO at different concentration are 2.1eV, 2.20eV and 2.23eV shown in figure 11. Presence of defects and oxygen vacancies decrease ZnO nanoparticles bandgap. Energy levels between valence band and conduction band due to these defects, which results reduction of energy values E_g . For the sake of defects analysis on the change of E_g values for ZnO, Band tail energy or urbach energy was taken into account. Defects can generates the band gape tailing in the band gape energy of ZnO [37].

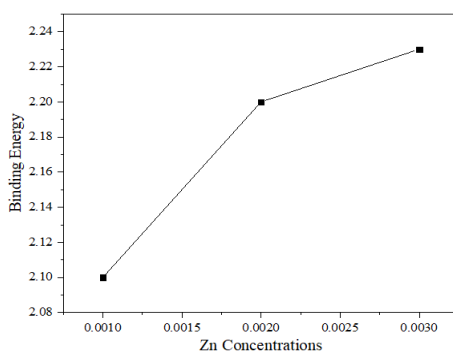


Fig. 10. Graph plotted of ZnO concentration against band gape.

4. Conclusion

Zinc oxide have been successfully synthesized via chemical Co-precipitation method with three different zinc concentration samples. FTIR and XRD analysis showed sharp crystalline peaks of zinc concentrations (0.001-0.003) displayed the development of the hexagonal wurtzite structure. It is also observed that particle size linearly increases with increase of zinc concentration. The average crystalline size is estimated 19nm to 47nm. As the ZnO concentration is increased the crystalline size calculated from the Williamsons hall method is increased.

The value of strain (ϵ) is also increased by increasing the ZnO concentrations. The result of UV Spectra indicate that specimen had symbolic absorbance which ranges from of 300-500 nm. Significant increase in band gap energies is observed from 2.1 to 2.23 eV with increase in Zn concentration from 0.001 - 0.003. Bandgap of ZnO nanoparticles is decreased due to presence of defects and oxygen vacancies.

Acknowledgements

The authors are very grateful to *department of Mechanical, Mechatronics, and Manufacturing Engineering (New Campus KSK), University of Engineering and Technology, Lahore, Pakistan* and *Department of Physics, University of Agriculture Faisalabad, 38040 Faisalabad, Pakistan* for providing us opportunity to carry out this work.

References

- [1] U. Özgür et al., A comprehensive review of ZnO materials and devices **98**(4), 11 (2005).
- [2] R. Turton et al., Evaluation of zinc oxide sorbents in a pilot-scale transport reactor: sulfidation kinetics and reactor modeling **43**(5), 1235 (2004).
- [3] I. Rosso et al., Zinc oxide sorbents for the removal of hydrogen sulfide from syngas **42**(8), 1688 (2003).
- [4] H.-M. Lin et al., Electrode effects on gas sensing properties of nanocrystalline zinc oxide **10**(3), 465 (1998).
- [5] J. Xu et al., Grain size control and gas sensing properties of ZnO gas sensor **66**(1-3), 277 (2000).
- [6] C. J. A. F. M. Feldmann, Polyol-mediated synthesis of nanoscale functional materials **13**(2), 101 (2003).
- [7] M. Zheng et al., Fabrication and optical properties of large-scale uniform zinc oxide nanowire arrays by one-step electrochemical deposition technique **363**(1-2), 123 (2002).
- [8] R. Wu, C. J. M. R. B. Xie, Formation of tetrapod ZnO nanowhiskers and its optical properties **39**(4-5), 637 (2004).
- [9] Z.-S. Wang et al., A highly efficient solar cell made from a dye-modified ZnO-covered TiO₂ nanoporous electrode **13**(2), 678 (2001).
- [10] G. M. Hamminga, G. Mul, J. A. J. C. E. S. Moulijn, Real-time in situ ATR-FTIR analysis of the liquid phase hydrogenation of γ -butyrolactone over Cu-ZnO catalysts: A mechanistic study by varying lactone ring size **59**(22-23), 5479 (2004).
- [11] M. Curri et al., Colloidal oxide nanoparticles for the photocatalytic degradation of organic dye **23**(1-2), 285 (2003).
- [12] P. V. Kamat, R. Huehn, R. J. T. J. O. P. C. B. Nicolaescu, A “sense and shoot” approach for photocatalytic degradation of organic contaminants in water **106**(4), 788 (2002).
- [13] B. P. Seung, C. K. J. J. O. A. S. Yun, Photocatalytic activity of nanometer size ZnO particles prepared by spray pyrolysis **1001**(28), S473 (1997).
- [14] G. P. Fotou, S. E. J. C. E. C. Pratsinis, Photocatalytic destruction of phenol and salicylic acid with aerosol-made and commercial titania powders **151**(1), 251 (1996).
- [15] M. Takagi et al., Production of titania nanoparticles by using a new microreactor assembled with same axle dual pipe **101**(1-3), 269 (2004).
- [16] V. Vamathevan et al., Silver metallisation of titania particles: effects on photoactivity for the oxidation of organics **98**(1-2), 127 (2004).
- [17] R. Hong et al., Experimental investigation and particle dynamic simulation for synthesizing titania nanoparticles using diffusion flame **108**(3), 203 (2005).
- [18] M. Kitano, M. J. P. T. Shiojiri, Benard convection ZnO/resin lacquer coating—a new approach to electrostatic dissipative coating **93**(3), 267 (1997).
- [19] M. Singhai et al., Synthesis of ZnO nanoparticles for varistor application using Zn-substituted aerosol OT microemulsion **32**(2), 239 (1997).
- [20] T. Tsuzuki, P. G. J. S. M. McCormick, ZnO nanoparticles synthesised by mechanochemical processing **44**(8-9), 1731 (2001).
- [21] D. Mondelaers et al., Synthesis of ZnO nanopowder via an aqueous acetate–citrate gelation method **37**(5), 901 (2002).
- [22] M. S. Tokumoto et al., Catalysis and temperature dependence on the formation of ZnO nanoparticles and of zinc acetate derivatives prepared by the sol–gel route **107**(2), 568 (2003).

- [23] K. Okuyama, I. W. J. C. E. S. Lenggoro, Preparation of nanoparticles via spray route **58**(3-6), 537 (2003).
- [24] T. Sato et al., Structure and optical spectrum of ZnO nanoparticles produced in RF plasma **255**(3-4), 313 (2003).
- [25] R. Viswanathan et al., Formation of zinc oxide– titanium dioxide composite nanoparticles in supercritical water **42**(22), 5535 (2003).
- [26] Z. Rataboul et al., Synthesis and characterization of monodisperse zinc and zinc oxide nanoparticles from the organometallic precursor [Zn (C₆H₁₁)₂] **643**, 307 (2002).
- [27] H. Zhang et al., Low temperature synthesis of flowerlike ZnO nanostructures by cetyltrimethylammonium bromide-assisted hydrothermal process **108**(13), 3955 (2004).
- [28] B. Liu, H. C. J. J. o. t. A. C. S. Zeng, Hydrothermal synthesis of ZnO nanorods in the diameter regime of 50 nm **125**(15), 4430 (2003).
- [29] X.-L. Hu et al., Sonochemical and microwave-assisted synthesis of linked single-crystalline ZnO rods **88**(2-3), 421 (2004).
- [30] R. J. C. J. P. E. Hong, Nanosized ZnO prepared by microwave homogeneous precipitation and its photocatalytic property **5**, 693 (2005).
- [31] W. Yu et al., Catalytic synthesis and structural characteristics of high-quality tetrapod-like ZnO nanocrystals by a modified vapor transport process **5**(1), 151 (2005).
- [32] Y. W. Koh et al., Self-assembly and selected area growth of zinc oxide nanorods on any surface promoted by an aluminum precoat. **108**(31), 11419 (2004).
- [33] J. H. Kim et al., Preparation of mono-dispersed mixed metal oxide micro hollow spheres by homogeneous precipitation in a micro precipitator **153**(3), 166 (2005).
- [34] R. Hong et al., Nanosized zinc oxide prepared by homogeneous precipitation and its photocatalytic property **23**(3), 231 (2005).
- [35] J. Wang, L. J. I. C. C. Gao, Synthesis and characterization of ZnO nanoparticles assembled in one-dimensional order **6**(7), 877 (2003).
- [36] E. Chikoidze et al., Electrical and optical properties of ZnO: Mn thin films grown by MOCVD **515**(24), 8519 (2007).
- [37] S. Klubnuan, S. Suwanboon, P. J. O. M. Amornpitoksuk, Effects of optical band gap energy, band tail energy and particle shape on photocatalytic activities of different ZnO nanostructures prepared by a hydrothermal method **53**, 134 (2016).